

# Study of Patchwelded Blanks Resistance Spot Welding (RSW) Before Hot Stamping with and without Heat Treatment Parameters

J. A. C. Lara<sup>a\*</sup> , L. Abbade<sup>a</sup>, C. S. Mucsi<sup>a</sup>, A. D. C. Nizes<sup>b</sup>, J. L. Rossi<sup>a</sup> 

<sup>a</sup>Instituto de Pesquisas Energéticas e Nucleares, Av. Prof. Lineu Prestes, 2242, Cidade Universitária, 05508-000, São Paulo, SP, Brasil.

<sup>b</sup>Thyssenkrupp Brasil - Springs & Stabilizers, Av. Abrahão Gonçalves Braga, 4, Vila Arapua, 04186-902, São Paulo, SP, Brasil.

Received: January 14, 2023; Revised: June 14, 2023; Accepted: July 16, 2023

In recent years, increasing automotive safety and energy efficiency has become a major concern in the automotive industry. Advanced high-strength steel (AHSS) was chosen for its weight reduction and high mechanical strength for the body in white (BIW). Specifically, it has been used in 22MnB5 steel press hardening type steel (PHS) with patchweld technology, which enables the production of reinforced and structural parts in a single stroke during the hot forming process. This study aimed to evaluate the resistance spot welding parameters for patchweld before hot stamping, considering the minimum and maximum residual stress, while ensuring a welding nugget diameter within the approved range. Microhardness and X-ray diffraction were used to analyze the welding zones for phase identification and residual stress measurements. After five weeks of elapsed time, the spot weld showed cracks that were not seen immediately after welding and were probably due to a high residual stress state.

**Keywords:** resistance spot welding, 22MnB5 steel, cold crack, patch weld, PHS.

## 1. Introduction

New advanced high-strength steels (AHSS) are specified to decrease the weight and improve the crashworthiness of car body structures<sup>1</sup>. 22MnB5 steel (Usibor<sup>®</sup> 1500) is intended for use in automotive structural and safety components because of its attained tensile strength of 1500 MPa. These steels are designed to be heat-treated and then quenched during the hot stamping process, but patch work (patchweld) technology was developed to increase productivity. The patch work joins 22MnB5 steel with Al-Si metallic coating blanks using resistance spot welding (RSW), which is performed before the patch-reinforced blank is heated at full austenitization temperature, hot-formed, and then cooled in the die stamping press<sup>2</sup>. Patch-work technology efficiency is related to the resistance spot weld used to maintain the peak force and energy absorption<sup>1</sup>. However, there are few studies on the macro characteristics of spot-weld joints. Resistance spot welding is the main joining process in assembly lines, and a car typically contains thousands of spot welds. Thus, the performance of the structure depends not only on the mechanical properties of the steel blanks but also on the joining mechanical behavior.

Resistance spot welding presents some particular aspects in the case of AHSS spot welds, which are more sensitive to failure at the faying surface than conventional mild steels. Several works concluded that the fracture toughness of RSW depends on the diameter of the nugget, the thickness of the sheet, the tensile breaking load, the welding time, and the current<sup>3,4</sup>.

Currently, international standards specify the minimum weld nugget size required to obtain the pull-out mode as follows: according to AWS D 8.9 M<sup>5</sup>, it is determined the minimum weld nugget size specified following Equation 1:

$$D = 4 t^{0.5} \quad (1)$$

where  $D$  is the weld-nugget size and  $t$  is the thinner sheet thickness (in mm).

For the Japanese JIS Z 3140:2017<sup>6</sup> and German DIN - DVS 2902-3<sup>7</sup> standards, the minimum required weld nugget size is specified following Equation 2:

$$D = 5 t^{0.5} \quad (2)$$

The AHSS suffers an interfacial mode failure that occurs through the nugget mainly because of the high hardness of the melting zone or internal shrinkage defects, whereas the pullout failure mode occurs by complete (or partial) nugget detachment from the joined sheet. The strength and failure behavior of spot weld joints under certain loading modes have been investigated in several studies, including full and partial interfacial failures (FIF and PIF, respectively for short), pullout failure (PF), and round button failure modes<sup>8</sup>. The load-bearing capacity and energy absorption capability of welds that fail under the overload interfacial mode are lower than those of welds that fail under the overload pullout mode<sup>9</sup>.

The welding schedules of mild steel with the same thickness follow the recommendations for high-strength steels (HSS)<sup>10</sup>: increase the electrode pressing force by 20% or more depending on the yield strength; increase the weld time when appropriate; try a multi-pulse welding schedule (several pulses or post heating); increase the tip diameter and/or change the type of electrode; and increase the minimum weld size.

\*e-mail: josecastillo@uol.com.br

The single-pulse welding schedule yielded average residual stress measurements smaller than the average of the welding schedule with a double pulse. The resistance welding parameters with pulse and post-weld heat treatment showed a hardness reduction in the subcritical heat-affected zone (SCHAZ) of 22MnB5 steel with an Al-Si coating patchweld, and the welding parameters with pulse and heat treatment showed cold cracks through the welding nugget<sup>11</sup>.

A phenomenon in materials science and engineering known as hydrogen embrittlement is characterized by a decrease in the ductility and fracture toughness of metals and alloys when hydrogen atoms are present. Hydrogen migrates and gathers at defect sites like grain boundaries or dislocations when it is introduced into a metal lattice. Even under very moderate applied stress, this hydrogen atom buildup can result in internal pressure that can eventually result in microcracks and brittle fracture. Electroplating, welding, and corrosion are just a few of the industrial processes that can result in hydrogen embrittlement. For metal components and structures in a variety of sectors to maintain structural integrity and dependability, hydrogen embrittlement must be understood and minimized. According to Costin et al.<sup>12</sup> *apud* Yurioka and Suzuki<sup>13</sup> there is a general agreement in the literature that hydrogen-assisted cold crack (HACC) formation requires the simultaneous presence of a critical hydrogen concentration, critical triaxial tensile stress levels, and a crack-susceptible microstructure. Hydrogen uptake is an essential requirement for hydrogen-assisted cracking (HAC)<sup>14</sup>.

As expected, hot-stamping steel, characterized by a completely martensitic microstructure and very high strength levels (ultimate tensile strength (UTS) of approximately 1600 MPa), shows a very high embrittlement index. The degradation of mechanical properties is marked; for example, the strength of a notched specimen with a hydrogen concentration of approximately 9 ppm (mass parts per million) is approximately 400 MPa, with a strength reduction of more than 75%<sup>15</sup>.

This study aimed to evaluate the resistance spot welding parameters for patchweld before hot stamping, considering the minimum and maximum residual stress, while ensuring a welding nugget diameter within the approved range. The 22MnB5 steel Al-Si coating on the patchweld before hot stamping showed a martensite microstructure in the fusion zone owing to the welding process and ferrite and perlite outside the welding zone before hot stamping. After hot stamping, the welding zone and base material undergo austenitization. Therefore, it was necessary to study the influence of residual stress on welding nuggets prior to hot stamping.

## 2. Material and Methods

The material selected in this study was 22MnB5 steel with Al-Si coating press-hardening steel before hot stamping. The thickness of the steel sheets used was 1.3 mm. Table 1 shows the chemical composition (% mass) of steel 22MnB5 steel in the as-received condition measured using fluorescence spectrometry of X-rays by energy dispersion (EDXRFS). The microstructure of as-received 22MnB5 steel with an Al-Si coating is composed of ferrite and a small amount of pearlite, while 22MnB5 steel has an Al-Si metallic coating and an intermetallic compound layer (IMC) of Fe<sub>2</sub>Al<sub>3</sub> resulting from diffusion during the hot dipping process, which is formed between the coated layer and the substrate<sup>16</sup>.

The recommended resistance welding parameters for welding AHSS include pre-burn (creation of nucleation points), pulse (cycling welding current), and post-weld heat treatment (heating the welding with a current at a time), resulting in an average microhardness of 463 HV0.5, with a variable rate of 6% in the fusion zone<sup>9</sup>. The welding parameters were based on a preceding optimization of the welding process<sup>11</sup>, and the detailed welding schedules are tabulated in Table 2.

The welds were performed on a “C” gun type medium frequency, dc inverter spot welder with Cu-Cr dome radius type electrode (ISO 5821-2009)<sup>17</sup> under a constant water cooling rate of 6 L.min<sup>-1</sup>. To accurately evaluate the nugget diameter, a resistance spot welding TESSONIC F1 ultrasonic inspection analyzer was used to verify the diameter and soundness of the resistance spot weld according to JIS Z 3140:2017<sup>6</sup> and German DIN - DVS 2902-3<sup>7</sup> standards. The probe of the ultrasonic equipment was positioned at the surface of the spot weld on both sides and showed a C-scan image.

The spot welds were cross-sectioned, mounted in Bakelite, polished with sandpaper grits P220, P400, P600, and P1200, and final polishing using alumina suspension (0.05 μm), and etched with Lepera reagent. The microstructures were observed using optical microscopy, and microhardness measurements were performed on the cross-section of spot welds in the fusion zone (FZ), upper critical heat-affected zone (UCHAZ), intercritical heat-affected zone (ICHAZ), subcritical heat-affected zone (SCHAZ), and base metal (BM) using a micro-Vickers hardness QATM Qness 60A+ EVO tester at an applied load of 500 gf and a dwelling time of 10 s. The parameters utilized in the equipment operational system for the XRD residual stress measurements RIGAKU Automate II are listed in Table 3.

The residual stress value resulting from the analysis represents the average deformation of the scanning area. These deformations can be measured in preferential directions, particularly when there is a need to visualize the residual stresses that can positively or negatively impact certain project loads. For stress analysis, each spot weld was measured in two different directions in relation to the longitudinal axis of the specimens: 0° and 90°. The width of the X-ray beam was 20 mm. To measure only the internal area of the spot weld and exclude the external areas, it was necessary to isolate the surrounding areas with Pb tape.

**Table 1.** Chemical composition of the boron-manganese steel, 22MnB5 steel grade (mass %), fluorescence spectrometry of X-rays by energy dispersion (EDXRFS).

Element	Amount
Al	0.030
B	0.002
C	0.230
Cr	0.160
Mn	1.180
N	0.005
Ni	0.120
Si	0.220
Ti	0.040
Fe	Bal.

Source: author.

**Table 2.** Resistance spot welding parameters used from the previous work<sup>11</sup>.

Test	Welding parameters									
	Squeeze (pre-burn)			Welding			Heat treatment		Hold	Pressure
	Current (kA)	Time (ms)	Ramp up	Pulse	Current (kA)	Time (ms)	Current (kA)	Time (ms)	Time (ms)	(kN)
P.1	5.0	60	50	NA	9.0	390	NA	NA	225	3.0
P.2	7.0	60	50	NA	9.0	390	NA	NA	225	3.0
P.3	5.0	100	50	NA	9.0	390	NA	NA	225	3.0
P.4	7.0	100	50	NA	9.0	390	NA	NA	225	3.0
P.5	7.0	100	50	NA	8.0	400	NA	NA	225	3.0
P.6	7.0	100	50	NA	8.5	400	NA	NA	225	3.0
P.7	7.0	100	50	NA	9.0	400	NA	NA	225	3.0
P.8	7.0	100	50	NA	9.5	400	NA	NA	225	3.0
P.9	7.0	100	50	2.0	8.5	200	NA	NA	225	3.0
P.10	7.0	100	50	2.0	9.0	200	NA	NA	225	3.0
P.11	7.0	100	50	2.0	9.5	200	NA	NA	225	3.0
P.12	5.0	100	50	2.0	9.3	200	6.0	100	225	3.0
P.13	7.0	100	50	2.0	9.3	200	6.0	100	225	3.0
P.14	5.0	100	50	2.0	9.3	200	8.0	120	225	3.0
P.15	7.0	100	50	2.0	9.3	200	8.0	120	225	3.0

NA - not used. Source: author.

**Table 3.** X-ray diffractometer configuration used for the present work.

Radiation	Cr K $\alpha$
Filter	V K $\beta$
Scanning plan	Fe $\alpha$ (211)
Poisson's coefficient	0.29
Young modulus [MPa]	210000
2 $\theta$ angle range	149° a 161°
$\Psi$ angle tilts	0.0; 16.8; 24.1; 30.0; 35.3; 40.2; 45.0
2 $\theta$ uniform steps	0.40

Source: author.

### 3. Results

The resistance spot welding parameters schedule was designed to balance the heat input to produce a welding nugget with a similar size according to the standards (DIN-DVS 2902-3:1991<sup>7</sup>; JIS Z 3140:2017<sup>6</sup>). The minimum welding nugget diameter of 22MnB5 steel with a thickness of 1.3 mm according to the standards was calculated to be a minimum of 5.7 mm and maximum indentation of 20% of the total stack-up, 0.52 mm according to the standards (DIN - DVS 2902-3:1991<sup>7</sup>; JIS Z 3140:2017<sup>6</sup>).

Ultrasonic inspections were performed on both sides of the welding nugget to measure the nugget diameter and the indentation formed by the electrode. The comparable dimensions of the welding nugget diameter produced by different welding parameters enabled an assessment of the impact of the residual stress effect and microhardness.

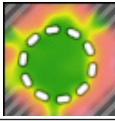
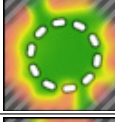
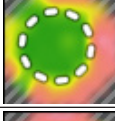
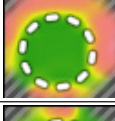
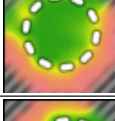
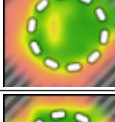
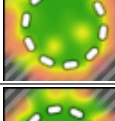
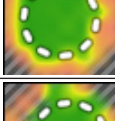
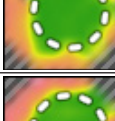
Table 4 shows the ultrasonic non-destructive inspection results in the resistance spot welding parameter schedules P2, P4, P6, P11, and P14 different welding nuggets. The ultrasonic inspection of the resistance spot welding parameter schedule

showed expulsion of the Al-Si coating around the welding nugget. The green areas are fused, and the red areas are not fused. The green image outside the dotted circle indicates the expulsion of the material during the resistance spot welding. Ultrasonic inspection of the resistance spot welding parameter schedule P6 showed an internal discontinuity (porosity) see table 4 moving electrode C-Scan.

The microstructure changed from the as-received condition to the FZ depending on the thermal gradient experienced during the resistance spot welding parameter. Five distinct zones were observed in the post-welded zones, which were categorized as 22MnB5 steel base metal (BM), subcritical HAZ (SCHAZ), intercritical HAZ (ICHAZ), upper critical HAZ (UCHAZ), fusion line (FL), and fusion zone (FZ) (ISO 5821-2009)<sup>17</sup>. The microstructure observed within the solidify weld pool of resistance spot welding, according to the parameters represented by parameter P4, is shown in Figure 1.

The BM of the 22MnB5 steel before hot stamping consisted of typical ferrite and perlite for both base metals welded (zones identified with an "f"). The transition zone was formed between the BM and HAZ, which is referred to as the SCHAZ (zone "e"), and it is visible as a black shade in the half section of the weld nugget. In the SCHAZ, the microstructure experienced a temperature close to the Ac1 temperature line, and the BM ferrite and cementite microstructure and resistance spot welding parameters with pulse and post-heat treatments showed a hardness reduction in this area<sup>18</sup>. The next zone to the SCHAZ is called ICHAZ (zone "d"), where the temperature reached between the temperature of the Ac1 and Ac3 line (temperatures from Fe-C diagram), and the austenite phase is formed along the prior austenite grain boundary; the austenite phase is transformed into martensitic and/or bainite upon cooling till room temperature.

**Table 4.** The ultrasonic non-destructive inspection results of the resistance spot welding parameters schedule P2, P4, P6, P11 and P14.

RSW parameter	Welding nugget side	C-Scan	Nugget diameter [mm]	Indentation [mm]
P2	Stationary electrode		6.05	0.17
	Moving electrode		5.79	0.21
P4	Stationary electrode		6.08	0.2
	Moving electrode		5.99	0.25
P6	Stationary electrode		6.75	0.23
	Moving electrode		6.34	0.25
P11	Stationary electrode		6.29	0.29
	Moving electrode		6.19	0.31
P14	Stationary electrode		6.25	0.15
	Moving electrode		6.13	0.18

Source: author.

The zone beside the ICHAZ is the UCHAZ (zone “c”), where the temperature is well above the Ac3 temperature line called the fusion line (zone “b”); therefore, complete austenitization occurred. The fully austenitized microstructure was retransformed into a martensitic structure because of the high cooling rate involved in the RSW process, including FL and FZ (zone “a”)<sup>19</sup> In their extensive study, Ximenes et al.<sup>20</sup> investigated the influence of heating rate on the transformation temperatures Ac1 and Ac3 of 22MnB5 steel sheets coated with Zn-Fe (GA). Their findings suggest that these temperatures have an impact on the microstructures of the steel, which is likely to be observed in various areas of resistance spot welding.

Figure 2 shows the positions of microhardness measurements. Microhardness was measured to determine the effect of the resistance spot welding parameters in the heat-affected zone (Figure 3). The comparison showed that the differences between the fusion zone and the heat-affected zone did not produce significant differences in the resistance welding parameters. The resistance welding parameter P2 with a higher pre-burn or squeeze current and long current time with no pulse and post-heat treatment showed a microhardness reduction of 62 HV<sub>0.5</sub> below the average of the measurements at the fusion zone of 461 HV<sub>0.5</sub>. The reduction in the resistance welding parameter P2 was located at the UCHAZ near the fusion line.

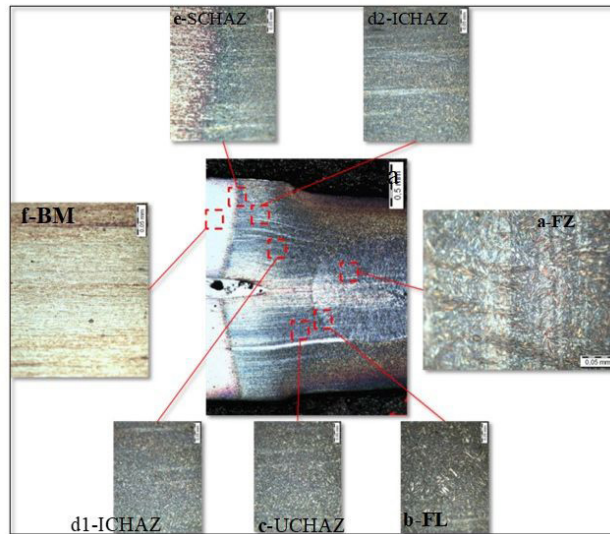


**Figure 1.** This figure shows the half cross section with different welding areas: a) FZ; b) FL; c) UCHAZ; d1) and d2) ICHAZ; e) SCHAZ and f) BM. Where, the cross-section of spot welds at fusion zone (FZ), upper critical heat affected zone (UCHAZ), inter critical heat affected zone (ICHAZ), subcritical heat affected zone (SCHAZ) and base metal (BM). Source: author.

A comparison of the intensity of the thermal cycle produced by no pulse (P3 and P6) showed the same level of microhardness along the welding zones. The resistance spot welding parameters (P11 and P14) showed a microhardness reduction in comparison with resistance spot welding (P2, P3, and P6) in the SCHAZ. P11 and P14 also showed differences in the SCHAZ welding zone, where P11 exhibited a lower microhardness reduction. The resistance spot welding parameter P14 with pulse and post-heat treatment showed a higher microhardness reduction in the welding zone SCHAZ. The temperature distribution result of the resistance spot welding parameters with pulse and/or pulse with post-heat treatment produced a wider HAZ.

Microhardness evaluation of the samples showed that the 22MnB5 steel with the Al-Si coating patch weld softened as the other AHSS, but the microhardness reduction depended on the resistance welding schedules. Because the resistance welding schedule is a group of parameters, for example, a higher welding current or even a longer welding time can affect the cooling time of the weld, and this different cooling time can result in hardness differences. The microhardness reduction observed in the samples welded with resistance spot welding parameters P11 and P14 was not related to the crack because the cold crack was far from the SCHAZ zone. The resistance spot welding parameter schedule P14 also showed a microhardness reduction at the ICHAZ near the UCHAZ with 43 HV<sub>0.5</sub> below the average of the measurements at the fusion zone.

According to Khanna and Long<sup>21</sup> results, it can be seen that the residual stress is tensile and maximum at the center of the weld and gradually decreases as the edge of the circular spot weld is approached. The maximum residual stress occurred at the center of the weld, had a magnitude of approximately 250 MPa (tensile), and was approximately in the radial direction. This study observed tensile residual stress with the same magnitude and even higher depending on the welding parameter.

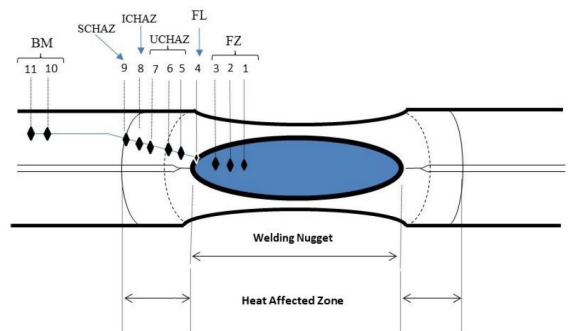


**Figure 2.** This figure shows the microhardness location in the cross sections of resistance spot welding. Source: author.

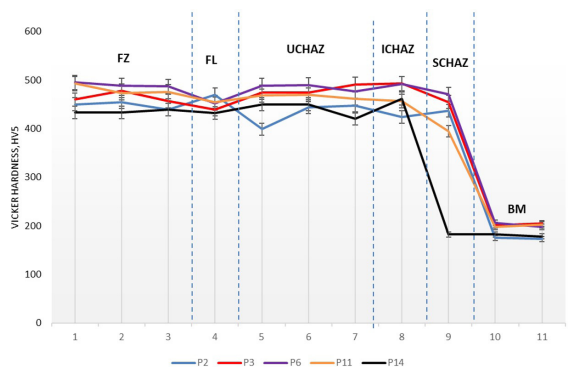


**Figure 3.** The figure shows microhardness on the cross sections of resistance spot welding for parameters without pulse (P2, P3 and P6), with pulse (P11) and post heat treatment (P14) into different welding areas: a- FZ; b- fusion line; c- UCHAZ; d1 and d2- ICHAZ; e-SCHAZ and f- BM. Where, the cross-section of spot welds at fusion zone (FZ), upper critical heat affected zone (UCHAZ), inter critical heat affected zone (ICHAZ), subcritical heat affected zone (SCHAZ) and base metal (BM). Source: author.

The welding schedule with pulse indicates that the welding current increases the residual stress, which is clear because higher residual stress measurements were obtained for welding parameters P11 and P12. In addition, parameter P11 showed a major difference between the two different directions to the longitudinal axis of the specimens. The post-weld treatments also showed higher values of residual stress, but the higher welding current at the post-weld treatment reduced the residual stress. This can be attributed to the stress release due to a lower cooling rate. Figure 4 shows the residual stress according to different welding parameters. The samples chosen for X-ray diffraction are indicated in Figure 5. The detrimental effect of H on the mechanical properties and diffusion of AHSS was specifically considered by some researchers<sup>15,21-25</sup> and fewer studies related to 22MnB5 steel press hardening steel are developed<sup>14</sup> and even less on 22MnB5 steel with Al-Si coating patch weld. However, the Vickers hardness results on the patchweld indicate the same possible behavior on the welding parameters used in this experiment.

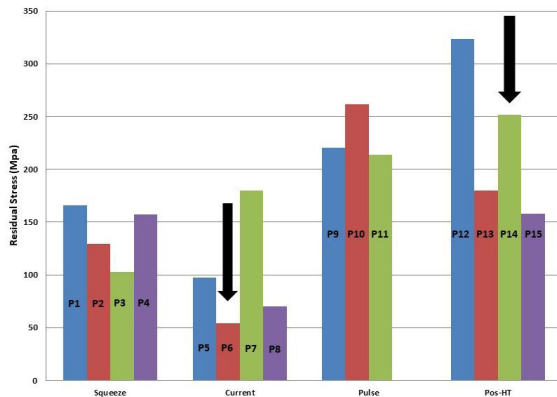


**Figure 4.** The figure shows that the residual stress varies according to different welding parameters. The samples chosen for X-ray diffraction are indicated with black arrows in the figure, that is, P6 and P14. The welding parameters were grouped into blocks based on the evaluated primary parameters. The first parameter of each group is denoted by the color blue, followed by the parameters in orange, gray, and yellow<sup>11</sup>. Source: author.

The resistance spot welding parameters schedule P14 with pulse and post heat treatment at the time of welding, cross-section cutting, and standard metallographic preparation. No cracks were detected in the coupons. The crack appeared five weeks later, and no polishing was performed to preserve the crack appearance, as shown in Figure 6. However, this crack could be assisted by hydrogen, and it is not completely ruled out as circumstantial evidence associated with a high residual stress and martensite microstructure and evidence from the literature<sup>12-14</sup>.

The Figure 7 shows two resistance spot welding nuggets obtained with the welding parameters. The same martensite microstructure was observed for the whole welding parameters. It is possible to assume that the fast cooling rate of the resistance spot welding produce the same microstructure in 22MnB5 steel with Al-Si coating before hot stamping.

Schmidová and Hanus<sup>24</sup> found out in their work that the quality of spot welding of safe auto parts can be decisively influenced by a non-homogeneous fusion zone. Specific heterogeneity was observed in some samples of operational weldments inside the weld metal. The formation of brittle intermetallic phases based on Al-Fe, as a consequence of the welding process, was observed. Aluminum and silicon melted in the Al-Si layer and were diluted in the weld metal during the cooling stage of welding. Both these elements are soluble in iron and are homogeneously distributed inside the solid solution but partially precipitated as an intermetallic phase along the fusion line<sup>26</sup>. Neither, Schmidová and Hanus<sup>24</sup>, nor Suehiro et al.<sup>26</sup> results were observed in the present study.

The X-ray diffraction was performed on the coupon with resistance spot welding parameter schedule P6 without pulse and heat treatment and lower residual stress in order to compare with a coupon with resistance spot welding parameter schedule P14 with pulse and heat treatment and higher residual stress.

The Figure 8a shows an X-ray diffraction results with ferrite and martensite content of the welding nugget made with resistance spot welding parameters P6. The Figure 8b shows a diffraction result with ferrite and martensite content at the welding nugget made with resistance spot welding parameters P14.

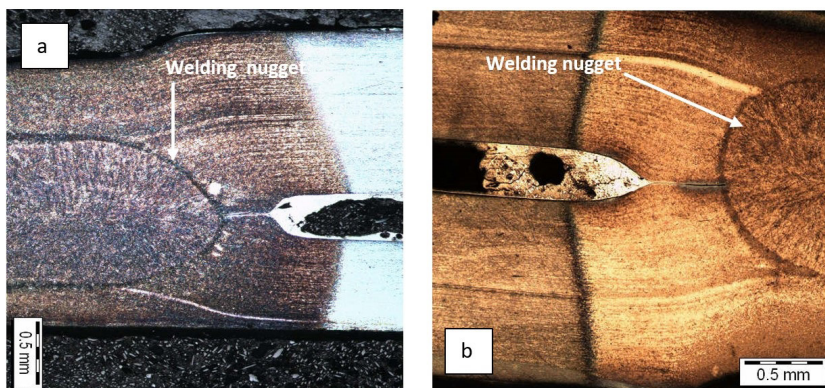


**Figure 5.** The figure showed cross-section of two nuggets obtained with the welding parameters. The Figure 5a is presented the welding nugget of the P2 welding parameter with low pre-burn time and the Figure 5b is the welding nugget of the P6 welding parameter with higher pre-burning without pulse or post heat treatment. Source: author.

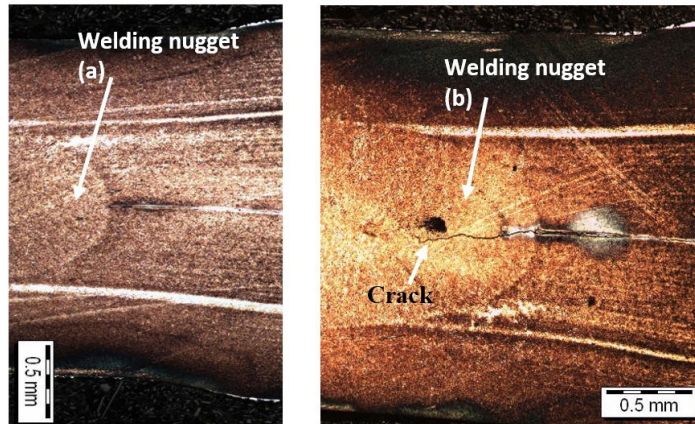


**Figure 6.** The figure shows optical micrographs on the cross sections of resistance spot welding for parameters with pulse and post heat treatment (P14) before (a) and after crack appears (b). The welding nugget welded with welding parameters P14 showed a crack through the fusion zone, see arrow, after five weeks of elapsed time. Source: author.

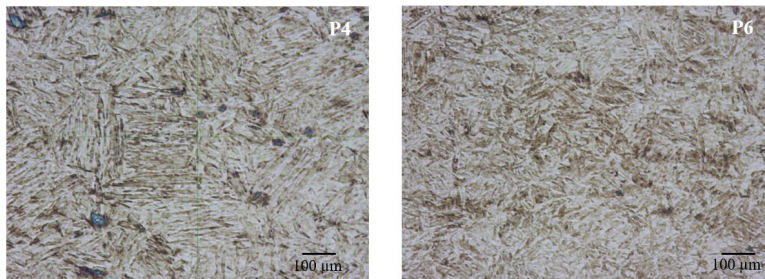


**Figure 7.** The welding nugget closed to the center of the P4 welding parameter where it can be observed the martensite phase. Optical micrographs of the welding nugget close to the edge of the fusion zone of the P6 welding parameter, it can be observed martensite throughout. Source: author.

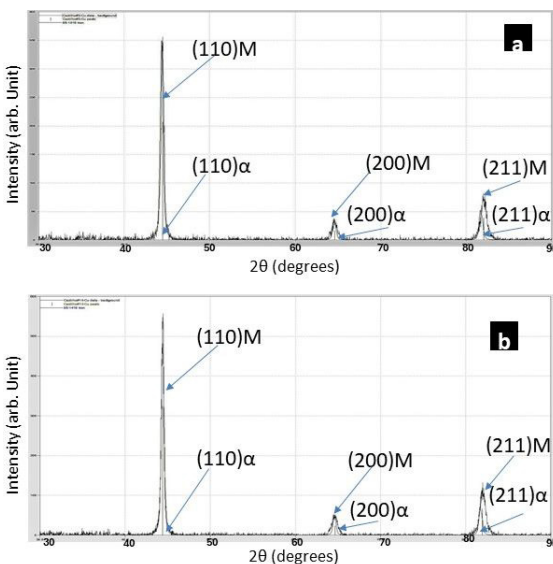


**Figure 8.** It is shown the X-ray diffraction on samples P6 (a) and P14 (b). In both samples it was detected martensite from the fusion zone of the resistance spot welding and ferrite from the HAZ. The difference in intensity between one diffractogram and another is due to the difference in the area exposed to the X-ray beam (in other words, sample size). Source: author.

The X-ray diffraction indicates the same microstructure of the fusion zone that can be the result of the cold crack susceptibility due to the high residual stress of resistance spot welding parameters P14<sup>11</sup>. In order to better illustrate Figure 8, the two screen images of the phase identification program (samples P6 and P14) showing that it was only possible to identify or find ferrite / martensite and no austenite or other phases could be observed. This does not mean that there cannot be austenite. Under the measurement conditions (small sample area, microstructure of the weld region and etc.) there may even be austenite below the detection limit of the method, but it is not possible to confirm or exclude it.

#### 4. Conclusion

On the basis of the experimental results, the following conclusions can be drawn. The ultrasonic welding nugget inspection resulted in no differences between the welding nugget diameters of the resistance spot welding schedule with balanced heat input. The results showed higher indentation and less fusion at the side of the moving electrode. The resistance spot welding parameters scheduled for 22MnB5 steel patchwork (patchweld) presented softening as the others AHSS. The softening at the HAZ was related with the welding parameters schedule.

The resistance spot welding schedule P2 showed a microhardness reduction and it was located at the UCHAZ near to the fusion line. The resistance spot welding schedule P11 and P14 with pulse result in microhardness reduction at the SCHAZ. Different resistance spot welding parameter can produce similar welding nugget with same pullout failure.

Considering the microhardness results for the different welding parameters, the crack was related to the high residual stress, martensitic microstructure observed on resistance welding parameters P14 (pulse and post heat treatment). The samples X-ray diffraction identification of ferrite and martensitic did not exclude other possible phases like austenite. The sample size and/or flatness could be affected the detection of other phases and other phases might be under the limit of the method.

## 5. Acknowledgments

The authors acknowledge CAPES for the Doctorate scholarship awarded to Lara, J. A. C.

## 6. References

- Billur E, editor. Hot stamping of ultra high strength steels: from a technological and business perspective. Turkey: Spring International Publishing; 2019, 245 p.
- Larsson JK, Lundgren J, Asbjörnsson E, Andersson H. Extensive introduction of ultra high strength steels sets new standards for welding in body shops. *Weld World*. 2009;53(5-6):4-14. <http://dx.doi.org/10.1007/BF03266709>.
- Ma C, Chen DL, Bhole SD, Boudreau G, Lee A, Birro E. Microstructure and fracture characteristics of spot welded DP600 steel. *Mater Sci Eng A*. 2008;485(1-2):334-46. <http://dx.doi.org/10.1016/j.msea.2007.08.010>.
- Marya M, Gayden X. Development of requirement for resistance spot welding dual-phase (DP600) steels Part 1-The cause of interfacial fracture. *Weld J*. 2005;84(11):172-85.
- American Welding Society. AWS D 8.9 M: recommended practices for test methods for evaluating the resistance spot welding behavior of automotive sheet steel materials. 3rd ed. Miami: AWS; 2012.
- Japanese Industrial Standard. JIS Z 3140:2017: method of inspection and acceptance levels for resistance spot welds (Foreign Standard). Japan: JIS; 2017.
- Deutsches Institut für Normung. DVS 2902-3: resistance spot welding of steels of an individual thickness of up to 3 mm; design and calculation. Berlin: DIN; 1991.
- Chao YJ. Ultimate strength and failure mechanism of resistance spot weld subjected to tensile, shear, or combined tensile / shear loads. *J Eng Mater Technol*. 2003;125(2):125-32. <http://dx.doi.org/10.1115/1.1555648>.
- Pouranvari M, Seyed MM. On the failure mode of M130 martensitic steel resistance spot welds. *Mater Technol*. 2013;47(6):771-6.
- Zhang H, Senkara J. Resistance welding: fundamentals and applications. 2nd ed. UK: CRC Press; 2017. 456 p.
- Lara JAC, Couto CP, Abbade L, Nizes AD, Gonzalez B, Colosio MA, et al. Effect of resistance spot welding parameters on the residual stress of automotive ultra high strength steel. In: 37th Senafor; 2017; Porto Alegre, Brazil. Proceedings. São Paulo: Instituto de Pesquisa Nuclear; 2017 [cited 2023 June 20]. p. 1-6. Available from: <http://repositorio.ipen.br/handle/123456789/34075>.
- Costin W, Lavigne O, Kotousov AG, Ghomashchi R, Brown IH, Linton V, et al. Susceptibility of acicular ferrite and upper bainite microstructures to hydrogen assisted cold cracking propagation. *Mater Sci Forum*. 2017;909:44-9. <http://dx.doi.org/10.4028/www.scientific.net/MSF.909.44>.
- Yurioka N, Suzuki H. Hydrogen assisted cracking in C-Mn and low alloy steel weldments. *Int Mater Rev*. 1990;35(1):217-49. <http://dx.doi.org/10.1179/imr.1990.35.1.217>.
- Kuhlmann M, Schwedler O, Holtschke N, Jüttner S. Consideration of hydrogen transport in press-hardened 22MnB5 steel. *Mater Test*. 2015;57(11-12):977-84. <http://dx.doi.org/10.3139/120.110808>.
- Couto CP, Politano R, Gomes MP, Colosio MA, Rossi JL. Diffusion analyses using GDOES technique of the 22MnB5 steel press hardened steel with Al-Si and Zn-Ni coatings. *Mater Sci Forum*. 2018;930:472-7. doi: 10.4028/www.scientific.net/MSF.930.472
- Lovicu G, Bottazzi M, D'aiuto F, Sanctis M, Dimatteo A, Santus C, et al. Hydrogen embrittlement of automotive advanced high-strength steels. *Metall Mater Trans, A Phys Metall Mater Sci*. 2012;43a(11):4075-87. <http://dx.doi.org/10.1007/s11661-012-1280-8>.
- International Organization for Standardization. ISO 5821-2009: resistance welding - spot welding electrode caps. Geneva, Switzerland: ISO; 2009.
- Lu Y, Peer A, Abke T, Kimchi M, Zhang W. Subcritical heat affected zone softening in hot-stamped boron steel during resistance spot welding. *Mater Des*. 2018;155(5):170-84. <http://dx.doi.org/10.1016/j.matdes.2018.05.067>.
- Betiku O, Shojaee M, Sherepenko O, Midawi ARH, Chertov AM, Ghassemi-Armaki H, et al. Optimizing post-weld performance of press-hardened steel resistance spot welds by controlling fusion zone porosity. *Weld World*. 2022;66:1733-46. <http://dx.doi.org/10.1007/s40194-022-01332-2>.
- Ximenes DAC, Moreira LP, Carvalho JER, Leite DNF, Toledo RG, Dias FMS. Phase transformation temperatures and Fe enrichment of a 22MnB5 steel Zn-Fe coated steel under hot stamping conditions. *J Mater Res Technol*. 2020;9(1):629-35. <http://dx.doi.org/10.1016/j.jmrt.2019.11.003>.
- Khanna S, Long X. Residual stresses in resistance spot welded steel joints. *Sci Technol Weld Join*. 2008;13(3):278-88. <http://dx.doi.org/10.1179/174329308X283884>.
- Abadi MMH, Pouranvari M. Failure-mode transition in resistance spot welded DP780 advanced high strength steel: effect of loading conditions. *Mater Technol*. 2014;48(1):67-71.
- Liu Q, Zhou Q, Venezuela J, Zhang M. A review of the influence of hydrogen on the mechanical properties of DP, TRIP, and TWIP advanced high-strength steels for auto construction. *Corros Rev*. 2016;34(3):127-52. <http://dx.doi.org/10.1515/correv-2015-0083>.
- Schmidová E, Hanus P. Weldability of Al-Si coated high strength martensitic steel. *Periodica Polytechnica Transport Engineering*. 2013;41(2):127-32. <http://dx.doi.org/10.3311/PPtr.7113>.
- Venezuela J, Liu Q, Zhang M, Zhou Q, Atrens A. A review of hydrogen embrittlement of martensitic advanced high-strength steels. *Corros Rev*. 2016;34(3):153-86. <http://dx.doi.org/10.1515/correv-2016-0006>.
- Suehiro M, Maki J, Kusumi K, Ohgami M, Miyakoshi T. Properties of aluminium-coated steels for hot-forming. Nippon Steel Corporation Technical Report. 2003;88:16-21.